Evidence for a Conformational Change in Actin Induced by Fimbrin (N375) Binding

Dorit Hanein,* Paul Matsudaira,‡ and David J. DeRosier*

*The W.M. Keck Institute for Cellular Visualization and The Rosenstiel Basic Medical Sciences Research Center, Department of Biology, Brandeis University, Waltham, Massachusetts 02254; and ‡Whitehead Institute of Biomedical Research and Department of Biology, Massachusetts Institute of Technology, Cambridge, Massachusetts 02142

Abstract. Fimbrin belongs to a superfamily of actin cross-linking proteins that share a conserved 27-kD actin-binding domain. This domain contains a tandem duplication of a sequence that is homologous to calponin. Calponin homology (CH) domains not only cross-link actin filaments into bundles and networks, but they also bind intermediate filaments and some signal transduction proteins to the actin cytoskeleton. This fundamental role of CH domains as a widely used actin-binding domain underlines the necessity to understand their structural interaction with actin. Using electron cryomicroscopy, we have determined the three-dimensional structure of F-actin and F-actin decorated with the NH_2-terminal CH domains of fimbrin (N375). In a difference map between actin filaments and N375-decorated actin, one end of N375 is bound to a concave surface formed between actin subdomains 1 and 2 on two neighboring actin monomers. In addition, a fit of the atomic model for the actin filament to the maps reveals the actin residues that line, the binding surface. The binding of N375 changes actin, which we interpret as a movement of subdomain 1 away from the bound N375. This change in actin structure may affect its affinity for other actin-binding proteins and may be part of the regulation of the cytoskeleton itself. Difference maps between actin and actin decorated with other proteins provides a way to look for novel structural changes in actin.

ANIMAL cells use ~25% of their total protein synthesis to construct the cytoskeletal structures involved in cellular motility, intracellular transport, exo- and endocytosis, locomotion, cellular polarity, anchorage, and cellular division. The actin-based cytoskeleton is a complex structure organized into bundles and networks by a large number of interacting proteins whose distribution and function have been characterized by a combination of microscopy, genetics, biochemistry, and immunology. One well-studied superfamily of actin cross-linking proteins shares a conserved 27-kD actin-binding domain (ABD),[1] and includes fimbrin, α-actinin, spectrin, dystrophin, ABP-120, and filamin (Dubreuil, 1991; Hartwig and Kwiatkowski, 1991; Matsudaira, 1991; Otto, 1994). The ABD itself represents a tandem duplication of a calponin-like sequence, which is referred to as a calponin homology (CH) domain (Castresana and Saraste, 1995). In addition to the role of CH domains in actin bundle and network formation, they are involved in connecting the actin cytoskeleton to intermediate filaments and in localizing signaling proteins to the interface between actin and the plasma membrane (Brown et al., 1995*a*,*b*; Castresana and Saraste, 1995). These CH domains have a critical role in the cell which can be better understood by elucidating their structural relationship to actin.

Fimbrin, the actin-binding protein of interest in this work, was first identified as a component of microvilli in intestinal brush border cells (Bretscher, 1981; Bretscher and Weber, 1980). It was later found to be present in a variety of cell types, where it is largely associated with polarized actin filaments in membrane ruffles, filopodia, stereocilia, and adhesion plaques (Bretscher, 1981; Bretscher and Weber, 1980; Glenney et al., 1981; Matsudaira and Burgess, 1979; Messier et al., 1993; Tilney and DeRosier, 1986; Tilney et al., 1980, 1989). Three highly homologous isoforms (I-, T-, and L-fimbrin) have been identified in humans (Anderson et al., 1985; Chapel et al., 1995; Goldstein et al., 1985; Lin et al., 1988, 1993, 1994). These isoforms display strict tissue specificity and distinct localization within the cells (Lin et al., 1994). Fimbrin is evolutionarily conserved

Address all correspondence to Dr. Dorit Hanein, W.M. Keck/Rosenstiel Center, Brandeis University, 415 South St. (MS-029), Waltham, Massachusetts 02254-9110. Tel.: (781) 736-2467. Fax: (781) 736-2419.

This paper is dedicated to the memory of Mary S. Tilney.

1. *Abbreviations used in this paper*: ABD, actin-binding domain; Actin-N375, α-rabbit skeletal muscle actin filaments decorated with the NH_2-terminal ABD of human T-fimbrin; CH, calponin homology; 3D, three dimensional; F-actin, α-rabbit skeletal muscle actin filaments; N375, NH_2-terminal ABD of human T-fimbrin (1–375 amino acids).

from *Saccharomyces cerevisiae* to humans, as indicated by its sequence and biochemical properties (Adams et al., 1991). Yeast mutants lacking fimbrin have abnormal actin cables, loose asymmetric distribution of cortical actin dots, and are defective in morphogenesis and endocytosis (Kubler and Riezman, 1993). Such mutants highlight the importance of fimbrin's role in the cell.

Sequence and proteolytic studies suggest that fimbrin structure and function is modular (de Arruda et al., 1990). Mild proteolysis cleaves fimbrin into a 12-kD NH_2-terminal regulatory domain (headpiece) and a 58-kD COOH-terminal actin–cross-linking fragment (core). Headpiece controls actin–cross-linking activity through its two calcium-binding domains. The fimbrin core consists of a tandem pair of 27-kD ABDs (Bretscher, 1981; Lin et al., 1994; Namba et al., 1992). Each ABD consists of a pair of CH domains. A genetic study using alanine-scanning mutants of actin suggests that yeast fimbrin binds actin subdomain 1 (Holtzman et al., 1994). In a complementary study, Honts et al. (1994) implicated a cluster of actin residues (32–100) directly involved in the interaction with fimbrin.

We can learn how fimbrin cross-links actin filaments by studying the interaction of its CH domains with α-rabbit skeletal muscle actin filaments (F-actin). In this study, we used electron cryomicroscopy and image analysis to determine the three-dimensional (3D) structure of actin decorated with the NH_2-terminal, actin-binding domain of human T-fimbrin (N375). N375 consists of the NH_2-terminal, calcium-binding headpiece domain and the adjacent of 27-kD ABD, which contains a pair of CH domains. In the map, one end of N375 binds the outer face of subdomains 1 and 2 of actin. Fitting the atomic model of F-actin (Lorenz et al., 1993) into the 3D maps shows that N375 contacts segments of polypeptide chain between residues 43–100 of one monomer and 146–148 and 350–355 of the adjacent monomer. These results are in agreement with genetic experiments (Holtzman et al., 1994; Honts et al., 1994). Moreover, N375 binding is accompanied by a conformational change of actin that appears to be a shift in subdomain 1. This shift might be necessary to generate the appropriate binding surface for N375. This is a novel conformational change that shows that actin-binding proteins do cause internal rearrangements of actin and therefore can potentially change the properties of actin.

Materials and Methods

Purification of Proteins

Recombinant Protein. N375 was constructed by amplifying residues 1–375 of human T-fimbrin and cloning the PCR product into pAB4. The cloned DNA was confirmed by sequencing. In short, freshly transformed BL21(DE3) cells were inoculated into 2× YT medium and grown at 25°C for 18 h. The cells were collected by centrifugation and frozen as a suspension in the presence of 25% glycerol. After a slow thaw and sonication, the lysed cells were centrifuged and the supernatant was dialyzed into 10 mM Tris, pH 8.0, 1 mM EDTA, 50 mM NaCl, 1 mM DTT, and 0.1 mM PMSF. The dialysate was loaded onto a DEAE-Sepharose Fast Flow column, and the protein was eluted with a 0.0–0.5-M linear NaCl gradient. N375-containing fractions were identified by SDS-PAGE and loaded on a Mono Q-sepharose (Q-Hi trap) column. Elution was accomplished with a 50–350-mM linear NaCl gradient. Fractions containing N375 were pooled and concentrated by centrifugation in a Centricon 30 (Amicon, Inc., Beverly, MA) ultrafiltration device. The protein was divided into 100-μl aliquots, flash frozen in liquid nitrogen, and stored at −80°C.

Actin. Rabbit skeletal muscle actin was prepared according to the method of Pardee and Spudich (1982), flash frozen in liquid nitrogen, and stored as 1-mg aliquots at −80°C. Before use, aliquots were thawed, dialyzed against G-actin buffer (2 mM Tris, pH 8.0, 0.2 mM $CaCl_2$, 0.2 mM ATP, 1 mM DTT), and clarified at 70 krpm for 30 min in a TLA-100 rotor (Beckman Instruments, Inc., Fullerton, CA). The actin was polymerized by addition of NaCl to 20 mM and $MgCl_2$ to 2 mM for 30 min at room temperature and stored on ice.

Preparation of N375-decorated F-actin

N375 (20–30 μM) was mixed with rabbit F-actin (10 μM) in 1 ml of binding buffer (10 mM Pipes, pH 7.0, 10–100 mM NaCl, 1 mM $MgCl_2$, 0.2 mM ATP, 0.1 mM EGTA). The sample was incubated for 1 h at room temperature and then processed for electron microscopy as described below. After every experiment, the mixture was pelleted at 60 krpm for 20 min in a Beckman TLA-100 rotor. Binding was determined by analysis of the supernatants and pellets by SDS-PAGE. Band densities were quantified from scanned images using the NIH Image software. For every experiment, we measured a 1:1 stoichiometry of N375 bound to F-actin.

Electron Microscopy

Frozen-hydrated specimens for electron cryomicroscopy were prepared as follows: a 4-μl drop of the sample was applied to air glow discharged holey carbon grids (400 mesh) in a humidified chamber. After 1 min of incubation, the grids were blotted and plunged in liquid nitrogen–cooled liquid ethane (Dubochet et al., 1988). The grids were stored under liquid nitrogen.

A cryotransfer system and cryoholder (model 626; both from Gatan Inc., Pleasanton, CA) were used to transfer the grids to a CM12 electron microscope (Philips Electronic Instruments Co., Mahwah, NJ) equipped with a Gatan anticontaminator (615N), a low dose kit, and Denka M3 LaB_6 filament (Denki Kagaku Kogyo Kaisha, Sibukawa, Japan). Low dose images were recorded using 120-kv electrons at a nominal magnification of 60,000, and ~2.2 μm defocus(electron dose ~10 $e^-/Å^2$). Kodak SO-163 plates were developed for 12 min in full-strength D19 developer (Eastman Kodak Co., Rochester, NY).

Image Analysis

Filament Alignment. Two data sets were analyzed in parallel: actin filaments (referred to as F-actin) and actin filaments decorated with the N375 construct (referred to as Actin-N375). Electron micrographs were screened both visually and by optical diffraction. Selected electron micrographs were digitized with an Eikonix 1412 densitometer (Eikonix Corp., Bedford, MA) at a scanning raster of 25 μm (~4.3 Å/pixel). Image display and analysis were performed on a Lexidata Lex 90 graphics device (Lexidato Corp., Billerica, MA) and a cluster of VAX color workstations. Electron density maps and atomic models were displayed on an Iris Indigo R4000 XS24 device (Silicon Graphics, Corp., Mountain View, CA) using O software (Jones et al., 1991).

Single filaments were selected for processing if they were over holes in the carbon film, reasonably straight, contained about ~100 subunits, and were well separated from neighboring filaments and from the edge of the carbon hole. Image processing and 3D reconstruction procedures used the Brandeis Helical Package as described previously (Owen et al., 1996).

Before computing Fourier transforms (512 × 4,096 pixels), digitized single filaments were corrected for curvature (Egelman, 1986), were tightly boxed, and the box edges were apodized (Stewart et al., 1981). For simplicity of nomenclature, we labeled layer lines as if the filament had 13 subunits in 6 turns. The true repeat is much longer, and there is no layer line overlap for the layer lines collected. The stronger layer lines were found to be (2,1), (−3,5), (−1,6), and (1,7), where the first of the pair of numbers is layer line order, n, and the second is layer line number, l. Positions of these layer lines were chosen interactively for each individual filament. A least squares fit of these strong layer lines was used to determine the positions of all the layer lines for that filament. Layer line data was collected to ~18 Å resolution.

The program SRCH1 (Morgan and DeRosier, 1992; Owen et al., 1996) was used to correct for phase origin and particle tilt using the algorithms described in DeRosier and Moore (1970). In short, SRCH1 operates by cross-correlation of an unaligned set of layer line data with a reference layer line data set. This procedure brings the unaligned data set to the same phase origin as that of the reference, and it calculates the root-mean-square (rms) amplitude weighted phase residual between the shifted data

and the reference (Amos and Klug, 1975). To determine the polarity (up vs. down orientation), the program repeats the alignment procedure with the filament turned upside down. A filament is included in the running average if its phase residual is <90° and the difference in phase residual between the up and down orientation is >8°. A total of 38 filaments of F-actin and 41 of Actin-N375 were submitted for alignment. Layer lines (2,1), (4,2), (−3,5), (−1,6), and (1,7) were used in the alignment of each data set. We blocked out near meridional data at a radius too small to have arisen from features in the structure. We used the strongest 5% of the remaining data on each layer line for alignment. We tested for out-of-plane tilts up to 10°. Statistically significant data in the averaged sets of Fourier coefficients were those for which $q \geq 2$ (Morgan et al., 1995; Owen and DeRosier, 1993). This ensures that the data included is significant at a 95.7% confidence level. To do the alignment and averaging, an initial reference layer line set was chosen from within each data set. After an initial average was calculated, this averaged layer line set was used as a new reference for the next cycle of alignment. After seven rounds of refinement, there were no significant changes in the values for tilt and shift in either data set.

The cumulative angular disorder, calculated as described in Stokes and DeRosier (1987), is 2.4° per subunit for the F-actin data set. The average filament length in the data set was 119 subunits. The coherence length of the filament for 2.4° is at least 2,280 subunits for the (1,7) layer line, at least 570 subunits for the (2,1), and 36 subunits for the (8,4) layer line.

The cumulative angular disorder is 3.2° per subunit for the Actin-N375 data set. The average filament length in this data set was 140 subunits. The coherence length of the filament for 3.2° is at least 1,282 subunits for the (1,7) layer line, at least 320 subunits for the (2,1) layer line, and 26 subunits for the (−7,3) layer line.

Cumulative angular disorder can be divided into two parts: a change in the twist of the filament and a noncumulative angular variation of the subunit positions about the average. A change in filament twist shifts the layer line positions from the expected positions. If the shift in layer line positions is small relative to their spacings, then the resulting changes in the observed amplitudes and phases will also be small and can be ignored. Because the shifts are small, ~1% of the unit cell, we did not correct the change in amplitudes and phases. Noncumulative variation reduces the coherence with which the subunits contribute to the layer line. This effect on coherence will reduce the amplitude but will not on average alter the phase. Thus, the amplitudes of the high order layer lines (e.g., $n = 8$) may be weakened, but the phases observed should be correct.

3D Reconstruction

The averaged layer line data sets were trimmed to a resolution of 28 Å. Since this is within the first node of the contrast transfer function, no phase correction was necessary. The abrupt edge in the data introduced by this procedure was smoothed to zero using a Gaussian falloff with a four-pixel half width. All layer line data too close to the meridian was discarded. Thus, the included layer lines had statistically significant Fourier coefficients that were reasonably symmetric about the meridian and followed the expected phase symmetry. 3D reconstructions were generated by Fourier-Bessel inversion of the averaged layer line data sets. 11 layer lines (including the equator) were used in the F-actin reconstruction. The axial position of the highest resolution layer line that had statistically significant Fourier coefficients is 1/(45 Å). 13 layer lines (including the equator) were used in the Actin-N375 reconstruction. The axial position of the highest layer line that had statistically significant Fourier coefficients was 1/(29 Å). Finally, these layer line data sets were separated into near-side and far-side data ($G_{n,l}(R)$). Thus, for each average layer line data set, F-actin and Actin-N375, two independent 3D reconstructions were computed. Particle boundaries were determined based on the predicted volume of the filament using a protein density of 0.81 D/Å^3 and a molecular mass of 82 kD per unit cell for Actin-N375. The F-actin maps presented in Figs. 2 *a*, 3, 4 *a*, and 5 have been contoured to match the actin portion of the decorated filaments to aid in the comparison of the structures.

Determination of Statistically Significant Features

For this analysis, we produced 3D density maps corresponding to the near- and far-sides of each of the individual data sets included in the average. After normalizing all maps so that the mean square densities were set to 1.0, we generated average maps and their corresponding variance maps (Trachtenberg and DeRosier, 1987). The significance of the details within each individual reconstruction was determined by performing a Student's *t* test (Morgan et al., 1995; Trachtenberg and DeRosier, 1987) for each pixel in the electron density maps at >99.99% confidence level. All the details in both the near and the far side maps of F-actin and Actin-N375 were significant by this criteria. Although the details in the near-side maps show the same structural information as the far-side maps, the far-side data is presented because it has significantly less noise.

The statistical analysis is carried out in real and reciprocal (Fourier) space. Independent estimates of variance for each voxel, which are best done in real space, are important because the variance may be different in different parts of the map. Variances measured in reciprocal space map into a constant estimate of variance in real space.

Statistical Significance of Features in the Difference Maps

The difference maps were obtained by subtracting either the far- or near-side of the F-actin map from the Actin-N375 map. Before subtraction, maps were aligned by a computer algorithm so the densities within the two maps overlap maximally. Alignments were carried out in real space and in reciprocal (Fourier) space. In reciprocal space, the alignment was done either using all common layer lines or using only the strong, common layer lines (layer lines 2, 4, −3, −1, 1, and 3). Using the strong, common layer lines gave the better alignment. The same alignment was achieved if done in real space. In this real space alignment (Hanein, D., and D.J. DeRosier, manuscript in preparation), the range of radii over which the alignment was carried out was limited to exclude all of the putative N375 portion of the map. Finally, we inspected the alignment visually to assure ourselves that the presence of the N375 did not result in a misalignment of the actin portions of the two reconstructions. No scaling of size was applied during the alignment or subtraction procedures. The biochemistry, microscopy, scanning, and image processing for both data sets were done under the exact same conditions. Variance maps were computed by combining the variances corresponding to the two average maps. The *t* maps were contoured to show differences significant at the 99.99% confidence level (Milligan and Flicker, 1987).

We used several approaches to generate difference maps to insure that the peak inside actin, which we interpret as a conformational change, was not an artifact. We generated difference maps using both reciprocal and real space data. We initially subtracted the two maps using the same set of layer lines for both data sets whether or not they included significant data (all the layer lines shown in Fig. 2, *b* and *d*). We cut off data beyond a resolution of 28 Å. Finding the difference peak within actin and fearing it might be caused by noise carried in by weak layer lines, we then restricted the maps by including only data that was statistically significant and then carried out the subtraction. Layer lines included (0,0), (2,1), (4,2), (6,3), (−7,3), (8,4), (−5,4), (−3,5), (−1,6), (1,7), and (3,8) for F-actin and (0,0), (2,1), (4,2), (6,3), (−7,3), (−5,4), (−3,5), (−1,6), (1,7), (3,8), (5,9), (7,10), and (−2,12) for Actin-N375. The peak remains. We also carried out the subtraction with common, strong layer lines (Layer lines included (0,0), (2,1), (4,2), (−3,5), (−1,6), (1,7), and (3,8)). The peak remains. We also tried carrying out the subtraction in reciprocal space using same set of layer lines or only the strong, common layer lines. The peak within actin was always present. The same is true of course for the peak we identify as arising from N375.

Results

Alignment and Averaging of Filaments

The Actin-N375 filaments (Fig. 1 *c*) are wider than the F-actin filaments (Fig. 1 *a*), which is a visual indication that N375 is present on the decorated filaments. Computed diffraction patterns of individual filaments are shown in Fig. 1, *b* and *d*. The four strongest layer lines used for layer line collection are marked with arrows. In general, diffraction patterns of individual decorated filaments showed stronger data on layer lines (2,1), (6,3) and (−5,4), again indicating the presence of N375.

Table I summarizes the results of alignment and averaging of the images in each of the data sets. The numerical values for the various parameters indicate that the data are good. The number of filaments and their lengths in

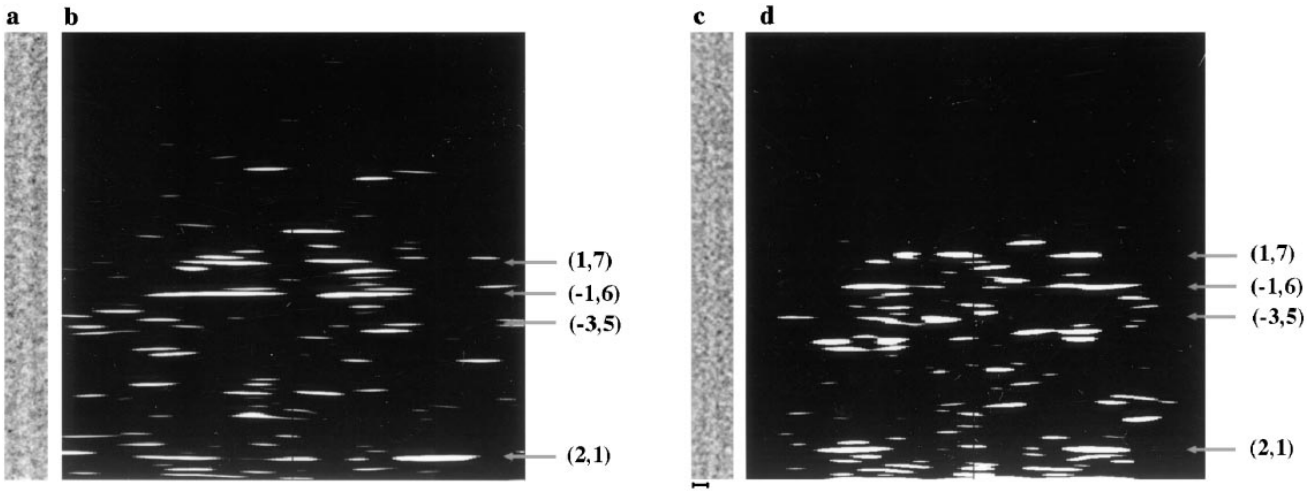

Figure 1. (*a*) An electron micrograph of an ice-embedded actin filament that was included in the average data set. (*b*) Computed electron diffraction pattern of the filament shown in *a.* (*c*) An electron micrograph of an ice-embedded actin filament decorated with N375 that was included in the average data set. (*d*) Computed electron diffraction pattern of the filament shown in *c.* The location of the strong layer lines are indicated by arrows. Bar, 100 Å.

subunits are typical of the number used for maps at this resolution (Bullitt et al., 1988; Egelman et al., 1982; McGough et al., 1994; Owen and DeRosier, 1993). The phase residuals reported here are lower than the ~40–60° residuals appearing in the reconstructions of others (Bullitt et al., 1988; Castellani et al., 1987; McGough et al., 1994; Orlova et al., 1994; Owen and DeRosier, 1993; Toyoshima and Wakabayashi, 1985). The up/down residual difference here, however, is comparable. Phase residual, which is a measure of the signal/noise ratio, is sensitive to how much of each data set is included in the determination. The lower the residual, the higher the signal to noise. The up/down difference in residuals, in contrast, is a measure of the polarity of the filaments and should depend on the structure more than the signal/noise ratio. The filaments of the two data sets individually cluster in the phase residual space, indicating that the averaging procedure included a uniform population of filaments with well-defined polarity.

Table I. Summary of Pertinent Information of the Two Average Data Sets

	F-actin	F-actin decorated with N375
Number of filaments in average	33 images	32 images
Number of subunits in average	3,922 subunits	4,356 subunits
Number of layer lines in average	10 layer lines	12 layer lines
Average phase residual	26°	33°
Average up/down difference	22°	27°
Number of subunits per turn	2.157 ($\sigma = 2.9 \times 10^{-3}$)	2.157 ($\sigma = 3.5 \times 10^{-3}$)
Average filament length (in subunits)	119 subunits	140 subunits
Cumulative angular disorder	2.4°	3.2°

The number of subunits per turn in the final reconstruction of F-actin is 2.157 ($\sigma = 2.886 \times 10^{-3}$) units in one turn of the 59-Å helix. The average helical symmetry in the final reconstruction of Actin-N375 has nearly identical helical symmetries, 2.157 subunits/turn ($\sigma = 3.483 \times 10^{-3}$). This value agrees with the reported helical symmetry values described by others (Egelman et al., 1982; McGough et al., 1994; Owen and DeRosier, 1993). The angular disorder ~3° is similar to that found by McGough et al. (1994) and Bullit et al. (1988), but is lower than the 5.2° determined by Egelman and DeRosier (1992) in negatively stained preparations. The lower value means that the filaments used for this study more closely approximate perfect helical symmetry.

In the averaged data sets (see Materials and Methods), a subset of the layer lines, trimmed radially to 28 Å, contained statistically significant information. Layer lines included (0,0), (2,1), (4,2), (6,3), (−7,3), (8,4), (−5,4), (−3,5), (−1,6), (1,7), and (3,8) for F-actin and (0,0), (2,1), (4,2), (6,3), (−7,3), (−5,4), (−3,5), (−1,6), (1,7), (3,8), (5,9), (7,10), and (−2,12) for Actin-N375. Between the common layer lines of the two data sets, the amplitudes of the Actin-N375 layer lines (6,3), (−5,4), (−3,5), and (2,1) increase by roughly a factor of two. All the remaining common layer lines have roughly comparable amplitudes.

3D Reconstructions

The surface presentation of F-actin (Fig. 2 *a*) shows the familiar features of an actin map, the two-stranded helical twist modulated by the mass of actin subunits. In all the reconstructions in this paper, the pointed end of the actin filament is up. The F-actin diameter is ~100 Å. In contrast, the Actin-N375 map contains extra density at the outermost edges of the filament and extends the filament diameter to ~115 Å (Figs. 2 *c*, 3, and 4 *b*, and *d*). This density is attributed to N375 bound to each actin subunit. The $G_{n,l}(R)$ of the far side averaged layer line is plotted for each data set (Fig. 2, *b* and *d*).

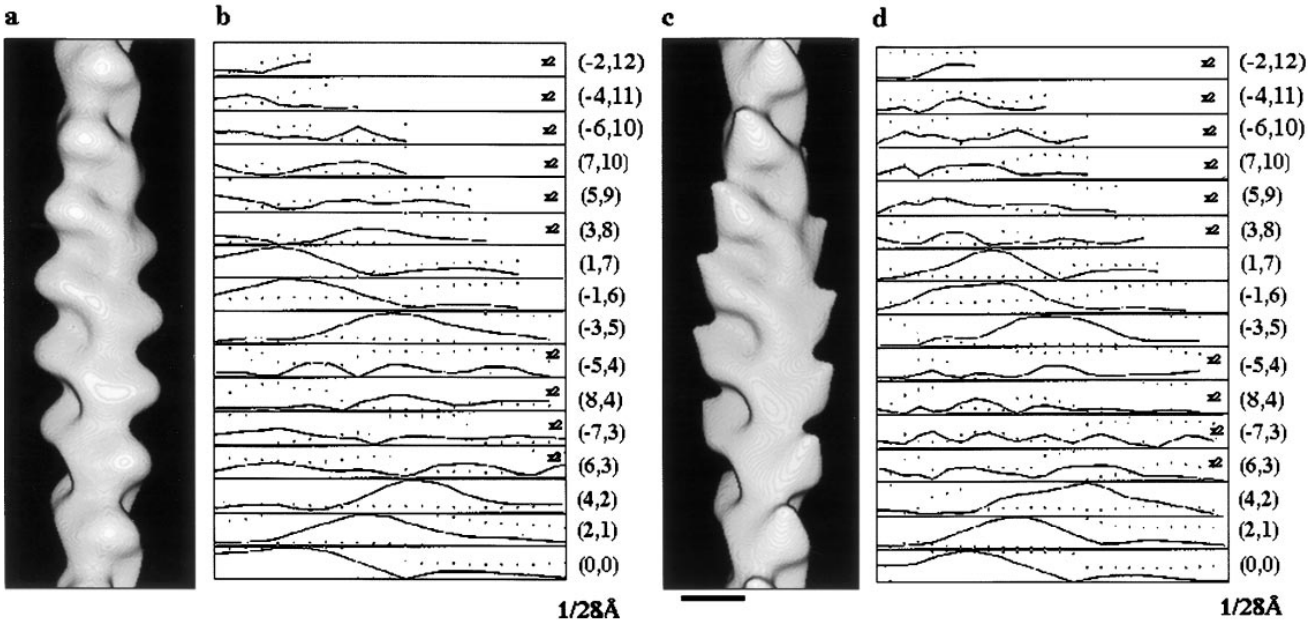

Figure 2. (*a*) Surface presentation of the average F-actin data set. (*b*) Plot of $G_{n,l}(R)$ amplitudes (*solid lines*) and phases (*dotted lines*) for the F-actin data set trimmed out to 28 Å. (*c*) Surface presentation of the average Actin-N375 data set. (*d*) Plot of $G_{n,l}(R)$ amplitudes (*solid lines*) and phases (*dotted lines*) trimmed out to 28 Å (*c*). For plotting purposes only, amplitudes of weak layer lines were scaled by a factor of 2 and are marked with 2×. In all reconstructions, the pointed end of the actin filament is up. Bar, 50 Å.

The F-actin/Actin-N375 Difference Map

Two positive difference peaks (bold contours) are seen in transverse sections through the difference map superimposed on the actin map (Fig. 3). The sections are spaced 4.3 Å apart in one asymmetric unit of the filament. For comparison, a surface view of the two positive peaks is shown in a stereo presentation in Fig 4 *d.* The first difference peak (*1* in Fig. 3) sits at the outer surface of the actin map. The density is kidney shaped with dimensions corresponding to ~50 × 25 × 25 Å. The dimensions are determined by the volume over which the difference is significant; it is not set to fit the expected volume of N375, for example. Peak 1 appears in Fig. 3, *a–c*, and it reappears on the other side of the actin filament in Fig. 3, *e*, *f*, and *g.* This region of extra density extends from actin subdomains 1 and 2. The variance corresponding to peak 1 is low (data not shown).

The second difference peak (*2* in Fig. 3) is located in the midst of the actin portion of the map, in the COOH-terminal region of subdomain 1, and is centered on residues 361–375 (Figs. 3, *a–c* and *g* and 4 *d*). The variance corresponding to peak 2 is also low (data not shown). Two areas of significant negative density are seen in the actin portion of the map (data not shown). One negative peak is located near subdomain 2, and the other negative peak is centered on the NH_2-terminal region of actin.

Discussion

N375 Density and Shape

The 3D structure of actin filaments and of actin filaments decorated with fimbrin N375 were determined using electron cryomicroscopy and helical reconstruction. A difference map, generated by subtraction of the two data sets either in real or reciprocal space, shows two positive peaks. Peak 1, which we interpret to be the N375 domain, is located outside the radius of actin, as is expected for a domain bound to actin. Furthermore, peak 1 has about the same dimensions as those of the fimbrin fragment 101–375 obtained by protein crystallography (Goldsmith et al., 1997). We interpret peak 2, which resides within the actin portion of the map, as a movement of subdomain 1 away from the bound N375 (further discussed below). Peak 1, which we refer to as N375, contacts a concave surface of the actin filament formed by subdomains 1 and 2 of one actin monomer and subdomain 1 of the neighboring monomer along the long-pitch helix. The contact region includes segments of polypeptide chain between residues 43–100 of one monomer and 146–148 and 350–355 of the adjacent monomer.

The ABDs of fimbrin and α-actinin share a conserved 27-kD sequence. We show that the kidney-shaped N375 measures ~50 × 25 × 25 Å. N375 is similar in size and shape to the ABD seen in the 2D maps of crystalline α-actinin (Taylor and Taylor, 1993). In their 2D maps, the ABD is subdivided into two peaks which are thought to correspond to the duplicated sequence that represents the CH domains. This interpretation is supported by the bilobed x-ray structure of the NH_2-terminal CH domains of T-fimbrin (Goldsmith et al., 1997). In this x-ray structure (determined to 2.1 Å resolution), a long, central helix connects two subdomains that are homologous in sequence and structure. Furthermore, N375 has the dimensions and shape of the x-ray structure (Goldsmith et al., 1997). Thus, different methodologies show consistently the same structure for these homologous ABDs.

Considering that N375 has two homologous CH domains,

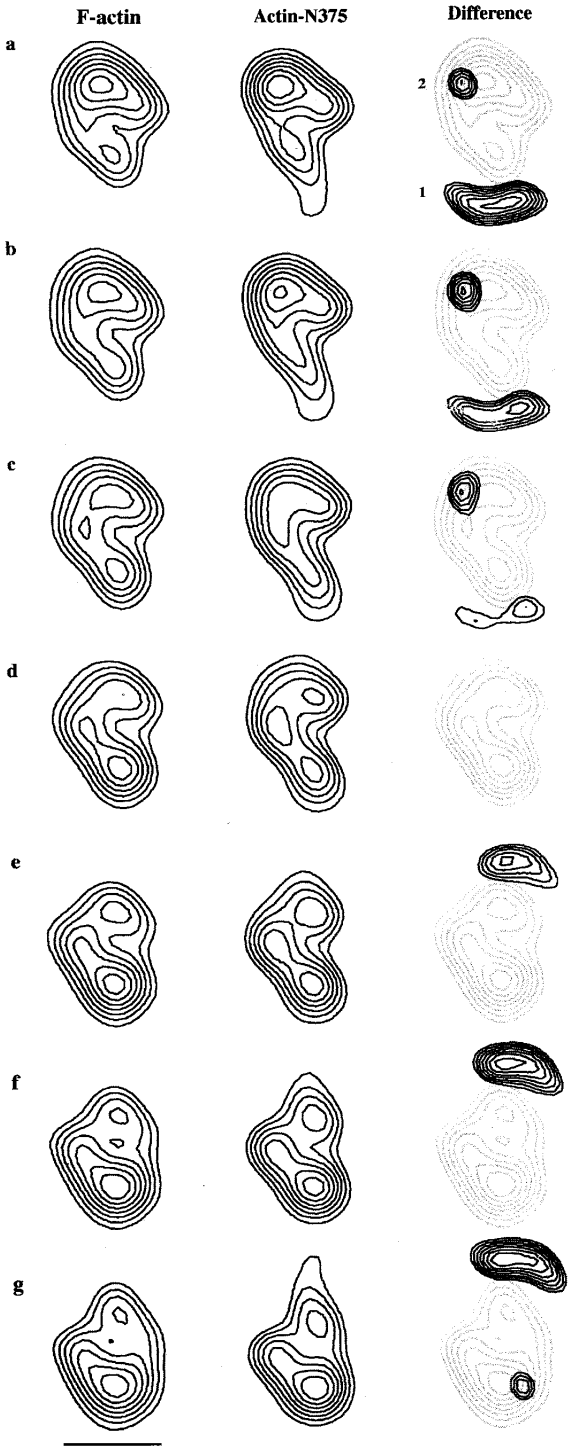

Figure 3. Sections through the F-actin reconstruction (*F-actin*) and the Actin-N375 reconstruction (*Actin-N375*). Sections are taken from the barbed end towards the pointed end. The sections are spaced 4.3 Å apart. The difference map between the two reconstructions is presented in the right column. The positive differences are contoured using black lines. Peak 1 corresponds to the N375 portion of the map, and peak 2 corresponds to the conformational change in subdomain 1. Contours corresponding to the actin map are superimposed on the difference contours. Contours start at the same density (4.0) in all maps. Contours are plotted at intervals of 6.3 in the F-actin and Actin-N375 maps and at intervals of 1.1 in the difference map. Bar, 50 Å.

we note in our map that actin appears to make contact toward one end of the elongated N375 structure (see difference map in Fig. 3). This end has a somewhat higher density, which we think is caused by the presence of the small calcium-binding domains. This suggests that the NH_2-terminal CH domain harbors the actin-binding site that measures ~25 × 20 Å.

N375 is much larger in the difference map than in the contoured decorated actin map (Figs. 3 and 4). In the reconstruction of Actin-N375, the density ascribable to N375 is much weaker than that ascribable to actin. The complication of weakened density is seen when the map is contoured for the expected volume of both the actin and N375, and actin is overrepresented and N375 underrepresented. The cause for the weakening of the density corresponding to N375 is uncertain, but loss of bound N375 during the blotting and plunging of grids is one possible explanation (Rost, L.E., D. Hanein, and D.J. DeRosier, manuscript in preparation). Indeed, there are other instances in which densities corresponding to the bound subunit on the decorated filaments are weaker than the density corresponding to the filament itself (Hirose et al., 1996; McGough et al., 1994; Orlova et al., 1994). The N375 is, however, correctly represented in a difference map in which the stronger peaks corresponding to actin are removed so that the map can be contoured to reveal the correct size and shape of N375.

Identification of Actin Residues at the Interface with N375

The first step in identifying the N375-binding site is to ensure that all maps share a common alignment. The 3D density maps were aligned by a computer algorithm so the densities within the maps overlap maximally. The alignment was done both in real and in reciprocal space (see Material and Methods). The alignment was checked visually to ensure that the extra density corresponding to the N375 did not force the program to compensate for the extra density by misaligning the actin portions of the maps relative to each other. The alignment of the atomic model of F-actin (Lorenz et al., 1993) to the prealigned density maps, however, was done manually using the program O (Jones et al., 1991). As seen in Fig. 4, the envelope encases the α-carbon backbone of actin, and all actin subdomains are readily identifiable. In the F-actin map, we see prominent density bridging subdomains 1 and 4 that is not seen in the atomic model at the same resolution. This bridge of density is reminiscent of the bridge seen in G-Ca^{++} actin (Fig. 6 *f* in Orlova and Egelman, 1995). However, our actin filaments were polymerized in the presence of NaCl, $MgCl_2$, and EGTA. In other 3D reconstructions (Bremer et al., 1991; Milligan et al., 1990; Orlova and Egelman, 1992, 1995; Owen and DeRosier, 1993), differences between the maps and the atomic model have been observed in the position of subdomain 2, but we do not find this difference.

When the actin filament atomic model is fitted to the difference map (Fig. 4 *d*), we see that N375 fits against a concave surface between two actin subunits. The putative contact region includes segments of the polypeptide chain between residues 43–100 of one monomer and 146–148

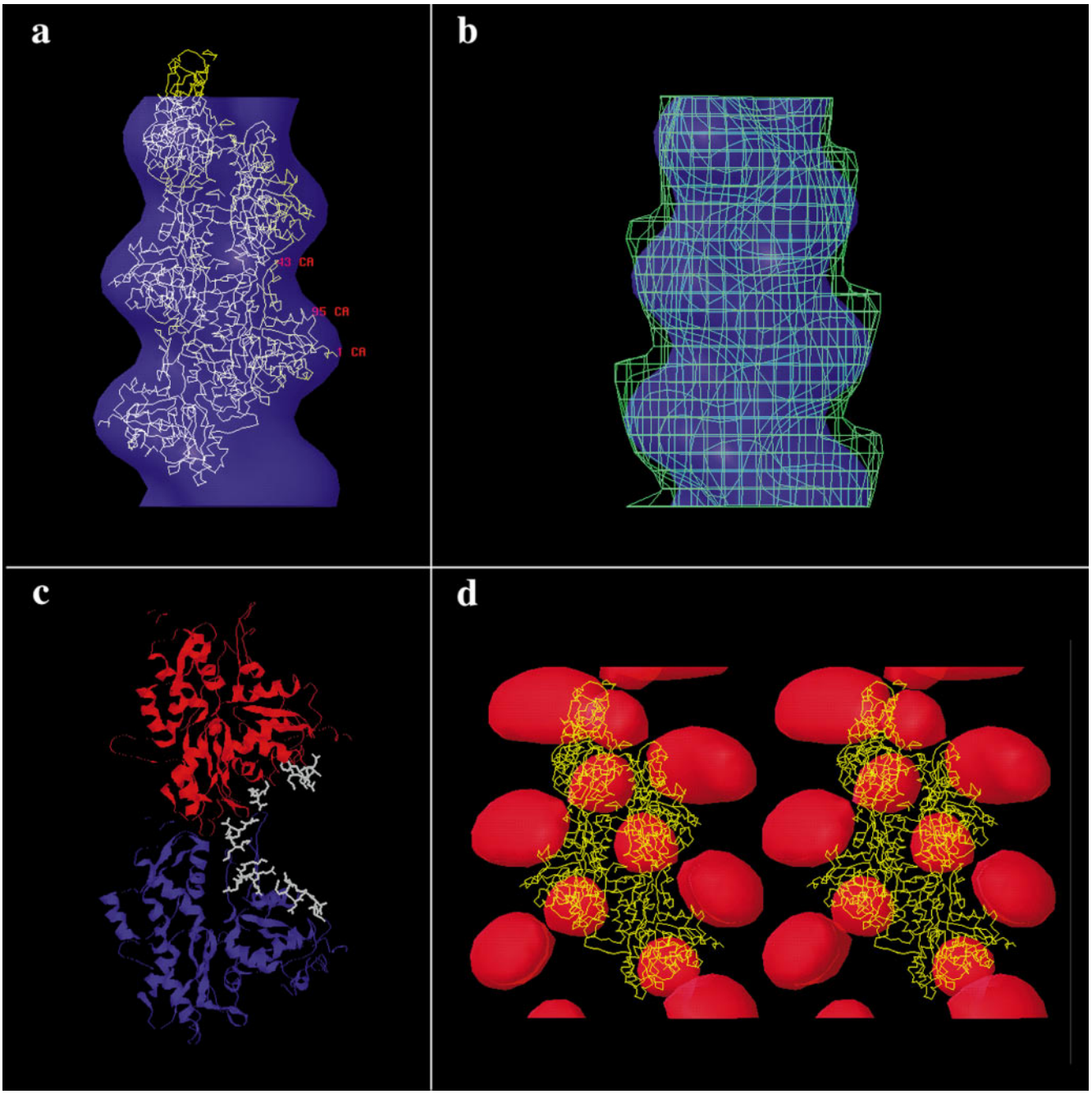

Figure 4. (*a*) Electron density map of F-actin overlaid with the atomic model of F-actin (Lorenz et al., 1993). (*b*) The Actin-N375 electron density map (*grid presentation*) displayed in alignment with the F-actin map. (*c*) Ribbon presentation of two actin monomers in which the proposed N375-binding site is highlighted. (*d*) Stereo presentation of the positive difference peaks arising from subtracting the F-actin map from the Actin-N375 map are shown together with the atomic model of F-actin. The outer density peak corresponds to N375, and the inner peak corresponds to a conformational change observed in actin upon N375 binding. In all maps, the pointed end of the actin filament is up.

and 350–355 of the adjacent monomer (Fig. 4 *c*). On the lower actin subunit, N375 appears to contact the loop built from residues Asn92-Pro98, the α-helix formed by residues Asp56-Lys61, and the loop containing residues Val43-Met48. On the upper actin monomer, the N375 contacts involve the loop-turn-loop structure formed by the residues Ser350-Met355.

Our structural observations provide a structural basis with biochemical and genetic studies on actin interactions with various members of this superfamily. These studies have identified actin residues 86–117 and 350–375 in subdomain 1 as likely binding sites for the 27-kD ABD of α-actinin, filamin, and dystrophin (Fabbrizio et al., 1993; Lebart et al., 1990, 1993; Levine et al., 1990, 1992; Mimura and Asano, 1987). Moreover, genetic analysis in yeast indicated that a cluster of actin residues 32–99/100 (Holtzman

et al., 1994; Honts et al., 1994; reviewed by Matsudaira, 1994) are involved in the interaction with fimbrin. Most of these residues lie at the outer surface of subdomains 1 and 2, and some of them appear to form extensive contacts with N375 in our reconstruction.

Changes in Actin Conformation on Binding of N375

The ionic conditions used for polymerization (Muhlrad et al., 1994; Orlova and Egelman, 1993; Orlova et al., 1995) and the presence of nucleotides (Lepault et al., 1994; Orlova and Egelman, 1992) or toxins (Drewes and Faulstich, 1993) all seem to have an effect on the actin conformational state. Although it seems highly likely that actin-binding proteins should also have an effect on the structure of actin itself, this has not been demonstrated. Owen and DeRosier (1993) suggested that subdomain 2 was shifted relative to the atomic model of F-actin, but this was based on a comparison of a map of the F-actin–scruin complex to the atomic model of the filament. Our comparison of Actin-N375 to F-actin provides more rigorous evidence for a change in actin conformation upon ABD binding. We compared the experimentally generated map of Actin-N375 to experimentally generated map of F-actin, and we see a change that we interpret as a shift of subdomain 1 upon N375 binding.

Our difference maps show a significant positive peak (2) centered at the COOH terminus of subdomain 1 (Figs. 3 and 4 *d*). This peak is unlikely to be an artefact resulting from noise in the images or from mishandling of the data for the following reasons: (*a*) The peak persists whether all the data or just the statistically significant data are included in the difference map. (*b*) The peak persists when the difference map is calculated in real (density) or reciprocal (Fourier) space. (*c*) The peak is present when an independent N375 data set is used and when an independent actin data set is used (data not shown). (*d*) The same peak has been found independently in studies of actin decorated with calponin (Hodgkinson et al., 1997), which has an ABD that is homologous to each of the two CH domains in N375. It is important to emphasize that calponin does not have the 12-kD calcium binding domain of N375 (the headpiece), eliminating the option that peak 2 is caused by the headpiece. Therefore, we must take the peak as a real feature of the difference map, which lies in the midst of the actin portion of the map. The variance in this region in both maps is low, suggesting that the shift is not the result of a change in the mobility of the domain. There are also two statistically significant negative regions in the difference map. One of them is centered near the NH_2 terminus of subdomain 1, and the other is located near subdomain 2. This information suggests that subdomain 1 is shifted outward and downward in a direction away from the bound N375 subunit (see Fig. 5).

Comparison with Actin Decorated with the CH Domain of α-Actinin (αA1-2)

N375 and α-actinin bind actin through similar if not identical mechanisms. Two pieces of evidence support this statement. First, the N375 difference peak is located at exactly the same place (within our resolution limits) as the αA1-2 ABD of α-actinin (McGough et al., 1994). The N375 peak

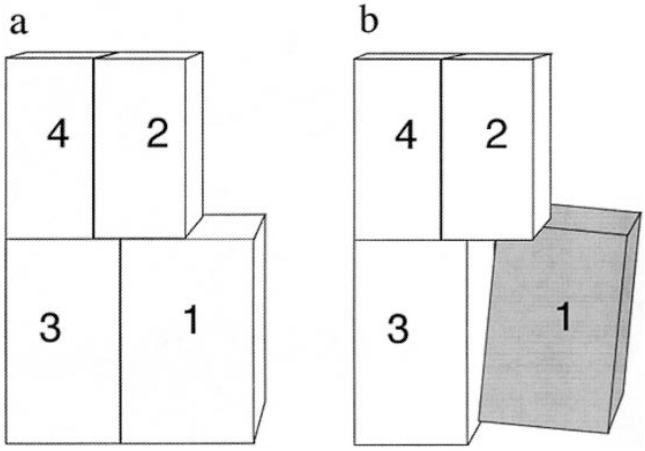

Figure 5. Schematic diagram of one actin subunit in the F-actin filament (*a*). The conformational change induced by N375 binding to F-actin is schematically presented in *b.* Subdomain 1 is shifted outward and downward in a direction away from the bound N375.

is also located at the same site as the calponin difference peak (Hodgkinson et al., 1997). Furthermore, the map of McGough et al. (1994), when aligned and compared to the Actin-N375, shows the same structural change in actin (Hanein, D., unpublished data), that we interpret as a shift in subdomain 1. The ABDs of the two proteins are homologous, and we would expect them to bind actin identically, but N375 includes an NH_2-terminal 12-kD calcium-binding domain. The presence of the calcium-binding domain in N375 may account for part of the shape difference seen between the two ABDs.

Our study provides significant new information in the mechanism of binding by CH domains in α-actinin and fimbrin. First, the actin residues at the interface with N375 are defined more precisely as described above. Second, actin interacts with a localized region on the side of N375. Presumably, this region corresponds to the three actin-binding sequences identified in ABP-120, filamin, α-actinin, and dystrophin (Bresnick et al., 1991; Levine et al., 1990, 1992). We are currently examining this binding site in more detail by fitting the x-ray structure to the EM difference map, and by evaluating the effects of point mutations in fimbrin on its actin-binding and cross-linking activities.

Conclusions

We have shown that one side of N375 binds actin through a concave surface that is formed by two actin monomers along the long-pitch helix. This binding also produces a conformational change that we interpret as a shift of subdomain 1 away from the bound N375. The effect of this change on the properties of actin is not known, but such a shift might be necessary to generate the appropriate binding surface for the N375 subunit, or it might alter the nucleotide-binding pocket which is located in the cleft between the inner and outer actin domains. Since actin dynamics and filament flexibility depend on the nucleotide state of actin, fimbrin binding is likely to be coupled with actin assembly or stability. Moreover, the change in actin

conformation may prevent other actin-binding proteins from binding to nearby sites on the same actin filament. This type of heretofore unobserved conformational shift may be a key element in the regulation of the actin cytoskeleton.

We thank Sharon C. Goldsmith and Steve C. Almo for providing the x-ray coordinates of fimbrin 101-375, Wenyan Shen for N375 construct, Matthew J. Footer for G-actin, W. Lehman and R. Craig for sharing their data before publication, and Amy McGough for the map of F-actin decorated with αA1-2. We would like to acknowledge the contributions made by Peter Vibert, David G. Morgan, Noreen Francis, Tanvir Shaikh, and Linda A. Melanson to this study. D. Hanein owes special thanks to Linda E. Rost for her extensive and valuable contributions throughout this work. P. Matsudaira acknowledges the contributions of W. Shen and F. Ziong to the construction of N375.

This work was supported by National Institutes of Health grant (GM26357) to D.J. DeRosier and CA44703 to P. Matsudaira.

Received for publication 4 November 1996 and in revised form 6 August 1997.

References

Adams, A.E., D. Botstein, and D.G. Drubin. 1991. Requirement of yeast fimbrin for actin organization and morphogenesis in vivo. *Nature (Lond.).* 354: 404–408.

Amos, L.A., and A. Klug. 1975. Three-dimensional image reconstructions of the contractile tail of T4 bacteriophage. *J. Mol. Biol.* 99:51–64.

Anderson, N.L., M.A. Gemmell, P.M. Coussens, S. Murao, and E. Huberman. 1985. Specific protein phosphorylation in human promyelocytic HL-60 leukemia cells susceptible or resistant to induction of cell differentiation by phorbol-12-myristate-13-acetate. *Cancer Res.* 45:4955-4962.

Bremer, A., R.C. Millonig, R. Sutterlin, A. Engel, T.D. Pollard, and U. Aebi. 1991. The structural basis for the intrinsic disorder of the actin filament: the "lateral slipping" model. *J. Cell Biol.* 115:689–703.

Bresnick, A.R., P.A. Janmey, and J. Condeelis. 1991. Evidence that a 27-residue sequence is the actin-binding site of ABP-120. *J. Biol. Chem.* 266:12989–12993.

Bretscher, A. 1981. Fimbrin is a cytoskeletal protein that cross-links F-actin in vitro. *Proc. Natl. Acad. Sci. USA.* 78:6849–6853.

Bretscher, A., and K. Weber. 1980. Fimbrin, a new microfilament-associated protein present in microvilli and other cell surface structures. *J. Cell Biol.* 86: 335–340.

Brown, A., G. Bernier, M. Mathieu, J. Rossant, and R. Kothary. 1995*a.* The mouse dystonia musculorum gene is a neural isoform of bullous pemphigoid antigen 1. *Nat. Genet.* 10:301–306.

Brown, A., G. Dalpe, M. Mathieu, and R. Kothary. 1995*b.* Cloning and characterization of the neural isoforms of human dystonin. *Genomics.* 29:777–780.

Bullitt, E.S., D.J. DeRosier, L.M. Coluccio, and L.G. Tilney. 1988. Three-dimensional reconstruction of an actin bundle. *J. Cell Biol.* 107:597–611.

Castellani, L., B.W. Elliott, Jr., D.A. Winkelmann, P. Vibert, and C. Cohen. 1987. Myosin binding to actin. Structural analysis using myosin fragments. *J. Mol. Biol.* 196:955–960.

Castresana, J., and M. Saraste. 1995. Does Vav bind to F-actin through a CH domain? *FEBS Lett.* 374:149–151.

Chapel, M.M., W. Shen, and P. Matsudaira. 1995. Sequential expression and differential localization of I-, L-, and T-Fimbrin during differentiation of the mouse intestine and yolk sac. *Dev. Dynamics.* 203:141–151.

de Arruda, M.V., S. Watson, C.S. Lin, J. Leavitt, and P. Matsudaira. 1990. Fimbrin is a homologue of the cytoplasmic phosphoprotein plastin and has domains homologous with calmodulin and actin gelation proteins. *J. Cell Biol.* 111:1069–1079.

DeRosier, D.J., and P.B. Moore. 1970. Reconstruction of three-dimensional images from electron micrographs of structures with helical symmetry. *J. Mol. Biol.* 52:355–369.

Drewes, G., and H. Faulstich. 1993. Cooperative effects on filament stability in actin modified at the C-terminus by substitution or truncation. *Eur. J. Biochem.* 212:247–253.

Dubochet, J., M. Adrian, J.-J. Chang, J.-C. Homo, J. Lepault, A.W. McDowall, and P. Schultz. 1988. Cryo-electron microscopy of vitrified specimens. *Q. Rev. Biophys.* 21:129–228.

Dubreuil, R.R. 1991. Structure and evolution of the actin cross linking proteins. *Bioessays.* 13:219–226.

Egelman, E.H., N. Francis, and D.J. DeRosier. 1982. F-actin is a helix with a random variable twist. *Nature (Lond.).* 298:131–135.

Egelman, E.H. 1986. An algorithm for straightening images of curved filamentous structures. *Ultramicroscopy.* 19:367–374.

Egelman, E.H., and D.J. DeRosier. 1992. Image analysis shows that variations in actin crossover spacings are random, not compensatory. *Biophys. J.* 63: 1299–1305.

Fabbrizio, E., A. Bonet-Kerrache, J.J. Leger, and D. Mornet. 1993. Actin-dystrophin interface. *Biochemistry.* 32:10457–10463.

Glenney, J.R., P. Kaulfus, P. Matsudaira, and K. Weber. 1981. F-actin binding and bundling properties of fimbrin, a major cytoskeletal protein of microvillus core filaments. *J. Biol. Chem.* 256:9283–9288.

Goldsmith, S.C., N. Pokala, W. Shen, A.A. Federov, P. Matsudaira, and S.C. Almo. 1997. The structure of an actin-crosslinking domain from human fimbrin. *Nat. Struct. Biol.* 4:708–712.

Goldstein, D., J. Djeu, G. Latter, S. Burbeck, and J. Leavitt. 1985. Abundant synthesis of the transformation-induced protein of neoplastic human fibroblasts, plastin, in normal lymphocytes. *Cancer Res.* 45:5643–5647.

Hartwig, J.H., and D.J. Kwiatkowski. 1991. Actin-binding proteins. *Curr. Opin. Cell Biol.* 3:87–97.

Hirose, K., A. Lockhart, R.A. Cross, and L.A. Amos. 1996. Three-dimensional cryoelectron microscopy of dimeric kinesin and ncd motor domains on microtubules. *Proc. Natl. Acad. Sci. USA.* 93:9539–9544.

Hodgkinson, J.L., M. El-Mezgueldi, R. Craig, P. Vibert, S.B. Marston, and W. Lehman. 1997. 3D image reconstruction of reconstituted smooth muscle thin filaments containing calponin. *J. Mol. Biol.* 273:150–159.

Holtzman, D.A., K.F. Wertman, and D.G. Drubin. 1994. Mapping actin surfaces required for functional interactions in vivo. *J. Cell Biol.* 126:423–432.

Honts, J.E., T.S. Sandrock, S.M. Brower, J.L. O'Dell, and A.E. Adams. 1994. Actin mutations that show suppression with fimbrin mutations identify a likely fimbrin-binding site on actin. *J. Cell Biol.* 126:413–422.

Jones, T.A., J.-Y. Zou, S.W. Cowan, and M. Kjeldgaard. 1991. Improved methods for the building of protein models in electron density maps and the location of errors in these models. *Acta Cryst. A.* 47:110–119.

Kubler, E., and H. Riezman. 1993. Actin and fimbrin are required for the internalization step of endocytosis in yeast. *EMBO J.* 12:2855–2862.

Lebart, M.C., C. Mejean, M. Boyer, C. Roustan, and Y. Benyamin. 1990. Localization of a new alpha-actinin binding site in the COOH-terminal part of actin sequence. *Biochem. Biophys. Res. Commun.* 173:120–126.

Lebart, M.C., C. Mejean, C. Roustan, and Y. Benyamin. 1993. Further characterization of the alpha-actinin-actin interface and comparison with filamin-binding sites on actin. *J. Biol. Chem.* 268:5642–5648.

Lepault, J., J.-L. Ranck, I. Erk, and M.-F. Carlier. 1994. Small angle X-ray scattering and electron cryomicroscopy study of actin filaments: role of the bound nucleotide in the structure of F-actin. *J. Struct. Biol.* 112:79–91.

Levine, B.A., A.J. Moir, V.B. Patchell, and S.V. Perry. 1990. The interaction of actin with dystrophin. *FEBS Lett.* 263:159–162.

Levine, B.A., A.J. Moir, V.B. Patchell, and S.V. Perry. 1992. Binding sites involved in the interaction of actin with the N-terminal region of dystrophin. *FEBS Lett.* 298:44–48.

Lin, C.S., R.H. Aerbersold, S.B. Kent, M. Varma, and J. Leavitt. 1988. Molecular cloning and characterization of plastin, a human leukocyte protein expressed in transformed human fibroblasts. *Mol. Cell Biol.* 8:4659–4668.

Lin, C.S., T. Park, Z.P. Chen, and J. Leavitt. 1993. Human plastin genes. Comparative gene structure, chromosome location, and differential expression in normal and neoplastic cells. *J. Biol. Chem.* 268:2781–2792.

Lin, C.S., W. Shen, Z.P. Chen, Y.H. Tu, and P. Matsudaira. 1994. Identification of I-plastin, a human fimbrin isoform expressed in intestine and kidney. *Mol. Cell Biol.* 14:2457–2467.

Lorenz, M., D. Popp, and K.C. Holmes. 1993. Refinement of the F-actin model against X-ray fiber diffraction data by the use of a directed mutation algorithm. *J. Mol. Biol.* 234:826–836.

Matsudaira, P.T., and D.R. Burgess. 1979. Identification and organization of the components in the isolated microvillus cytoskeleton. *J. Cell Biol.* 83:667–673.

Matsudaira, P. 1991. Modular organization of actin crosslinking proteins. *Trends Biochem. Sci.* 16:87–92.

Matsudaira, P. 1994. The fimbrin and alpha-actinin footprint on actin. *J. Cell Biol.* 126:285–287.

McGough, A., M. Way, and D. DeRosier. 1994. Determination of the α-actinin–binding site on actin filaments by cryoelectron microscopy and image analysis. *J. Cell Biol.* 126:433–443.

Messier, J.M., L.M. Shaw, M. Chapel, P. Matsudaira, and A.M. Mercurion. 1993. Fimbrin localized to an insoluble cytoskeletal fraction is constitutively phosphorylated on its headpiece domain in adherent macrophages. *Cell Motil. Cytoskeleton.* 25:223–233.

Milligan, R.A., and P.F. Flicker. 1987. Structural relationships of actin, myosin, and tropomyosin revealed by cryo-electron microscopy. *J. Cell Biol.* 105:29–39.

Milligan, R.A., M. Whittaker, and D. Safer. 1990. Molecular structure of F-actin and location of surface binding sites. *Nature (Lond.).* 348:217–221.

Mimura, N., and A. Asano. 1987. Further characterization of a conserved actin-binding 27-kDa fragment of actinogelin and alpha-actinins and mapping of their binding sites on the actin molecule by chemical cross-linking. *J. Biol. Chem.* 262:4717–4723.

Morgan, D.G., and D.J. DeRosier. 1992. Processing images of helical structures: a new twist. *Ultramicroscopy.* 46:263–285.

Morgan, D.G., C. Owen, L.A. Melanson, and D.J. DeRosier. 1995. Structure of bacterial flagellar filaments at 11 A resolution: packing of the alpha-helices. *J. Mol. Biol.* 249:88–110.

Muhlrad, A., P. Cheung, B.C. Phan, C. Miller, and E. Reisler. 1994. Dynamic

properties of actin. Structural changes induced by beryllium fluoride. *J. Biol. Chem.* 269:11852–11858.
Namba, Y., M. Ito, Y. Zu, K. Shigesada, and K. Maruyama. 1992. Human T cell L-plastin bundles actin filaments in a calcium-dependent manner. *J. Biochem. (Tokyo).* 112:503–507.
Orlova, A., and E.H. Egelman. 1992. Structural basis for the destabilization of F-actin by phosphate release following ATP hydrolysis. *J. Mol. Biol.* 227: 1043–1053.
Orlova, A., and E.H. Egelman. 1993. A conformational change in the actin subunit can change the flexibility of the actin filament. *J. Mol. Biol.* 232:334–341.
Orlova, A., X. Yu, and E.H. Egelman. 1994. Three-dimensional reconstruction of a co-complex of F-actin with antibody fab fragments to actin's NH_2 terminus. *Biophys. J.* 66:276–285.
Orlova, A., and E.H. Egelman. 1995. Structural dynamics of F-actin. I. Changes in the C terminus. *J. Mol. Biol.* 245:582–597.
Orlova, A., E. Prochniewicz, and E.H. Egelman. 1995. Structural dynamics of F-actin. II. Cooperativity in structural transitions. *J. Mol. Biol.* 245:598–607.
Otto, J.J. 1994. Actin-bundling proteins. *Curr. Opin. Cell Biol.* 6:105–109.
Owen, C., and D. DeRosier. 1993. A 13-A map of the actin-scruin filament from the limulus acrosomal process. *J. Cell Biol.* 123:337–344.
Owen, C.H., D.G. Morgan, and D.J. DeRosier. 1996. Image analysis of helical objects: the Brandeis helical package. *J. Struct. Biol.* 116:167–175.
Pardee, J.D., and J.A. Spudich. 1982. Purification of muscle actin. *Methods Enzymol.* 85 Pt. B:164–181.
Stewart, M., R.W. Kensler, and R.J. Levine. 1981. Structure of Limulus telson muscle thick filaments. *J. Mol. Biol.* 153:781–790.
Stokes, D.L., and D.J. DeRosier. 1987. The variable twist of actin and its modulation by actin-binding proteins. *J. Cell Biol.* 104:1005–1017.
Taylor, K.A., and D.W. Taylor. 1993. Projection image of smooth muscle α-actinin from two-dimensional crystals formed on positively charged lipid layers. *J. Mol. Biol.* 230:196–205.
Tilney, L.G., and D.J. DeRosier. 1986. Actin filaments, stereocilia, and hair cells of the bird cochlea. IV. How the actin filaments become organized in developing stereocilia and in the cuticular plate. *Dev. Biol.* 116:119–129.
Tilney, L.G., D.J. Derosier, and M.J. Mulroy. 1980. The organization of actin filaments in the stereocilia of cochlear hair cells. *J. Cell Biol.* 86:244–259.
Tilney, M.S., L.G. Tilney, R.E. Stephens, C. Merte, D. Drenckhahn, D.A. Cotanche, and A. Bretscher. 1989. Preliminary biochemical characterization of the stereocilia and cuticular plate of hair cells of the chick cochlea. *J. Cell Biol.* 109:1711–1723.
Toyoshima, C., and T. Wakabayashi. 1985. Three-dimensional image analysis of the complex of thin filaments and myosin molecules from skeletal muscle. IV. Reconstitution from minimal- and high-dose images of the actin-tropomyosin-myosin subfragment-1 complex. *J. Biochem. (Tokyo).* 97:219–243.
Trachtenberg, S., and D. DeRosier. 1987. Three-dimensional structure of the frozen-hydrated flagellar filament: the left-handed filament of *Salmonella typhimurium. J. Mol. Biol.* 195:581–601.